

Asymmetries in the simulated ozone distribution on TRAPPIST-1e due to orography

ANAND BHONGADE,¹ DANIEL R MARSH,^{2,3} FELIX SAINSBURY-MARTINEZ,² AND GREGORY COOKE^{2,4}

¹*School of Earth and Environment, University of Leeds, Leeds, UK*

²*School of Physics and Astronomy, University of Leeds, Leeds, UK*

³*School of Chemistry, University of Leeds, Leeds, UK*

⁴*Institute of Astronomy, University of Cambridge, UK*

ABSTRACT

TRAPPIST-1e is a tidally locked rocky exoplanet orbiting the habitable zone of an M dwarf star. Upcoming observations are expected to reveal new rocky exoplanets and their atmospheres around M dwarf stars. To interpret these future observations we need to model the atmospheres of such exoplanets. We configured CESM2-WACCM6, a chemistry climate model, for the orbit and stellar irradiance of TRAPPIST-1e assuming an initial Earth-like atmospheric composition. Our aim is to characterize the possible ozone (O_3) distribution and explore how this is influenced by the atmospheric circulation shaped by orography, using the Helmholtz wind decomposition and meridional mass streamfunction. The model included Earth-like orography and the substellar point was located over the Pacific Ocean. For such a scenario, our analysis reveals a North-South asymmetry in the simulated O_3 distribution. The O_3 concentration is highest below 10 hPa level (below \sim 30 km) near the South pole. This asymmetry results from the presence of land masses on the night side that cause drag in near-surface flows and lead to an asymmetric meridional overturning circulation. Catalytic species were roughly symmetrically distributed and were not found to be primary driver for the O_3 asymmetry. The total ozone column (TOC) density was higher for TRAPPIST-1e compared to Earth, with 8000 Dobson Units (DU) near the South pole and 2000 DU near the North pole. The results emphasize the sensitivity of O_3 to model parameters, illustrating how incorporating Earth-like orography can affect atmospheric dynamics and O_3 distribution. This link between surface features and atmospheric dynamics underlines the importance of how changing model parameters used to study exoplanet atmospheres can influence the interpretation of observations.

Keywords: Exoplanet atmospheres (487); Exoplanet atmospheric composition (2021); Exoplanet atmospheric dynamics (2307); Transmission spectroscopy (2133); James Webb Space Telescope (2291)

1. INTRODUCTION

Scientists have long wondered about the existence of life on other planets and this curiosity has motivated them to explore celestial bodies beyond our solar system. To date, over 5600 confirmed exoplanets have been identified by instruments like the Kepler Space Telescope, the Transiting Exoplanet Survey Satellite, and various space-based and ground-based telescopes.¹ Studies utilizing Kepler mission data have found that the presence of small rocky exoplanets around M dwarf stars exceeds that around Sun-like stars (Howard et al. 2012; Dressing & Charbonneau 2015; Mulders et al. 2015; Gaidos et al. 2016), although this is likely because of the observational bias of telescopes for detecting exoplanets around smaller, cooler and dimmer stars. To date, 200 confirmed rocky exoplanets have been detected.²

M dwarf stars, constituting approximately 70% of all known stars in our galaxy, have garnered scientific attention due to their abundance and compact planetary systems (Bochanski et al. 2010). The location of the habitable zone around a star depends upon its stellar properties (Huang 1959). M dwarf stars, characterized by their low temperature and flux, have habitable zones situated closer to them. Detection methods such as transit photometry and radial velocity

¹ https://exoplanetarchive.ipac.caltech.edu/docs/counts_detail.html - Date: 15/04/2024

² <https://exoplanets.nasa.gov/what-is-an-exoplanet/planet-types/terrestrial/> - Date: 15/04/2024

rely on the planet-to-star mass and size ratio, making the search for rocky exoplanets in habitable zones around M dwarf stars more feasible due to the star's relatively small size (Shields et al. 2016; Reiners et al. 2018; Gould et al. 2003; Nutzman & Charbonneau 2008).

Exoplanets orbiting M dwarfs can be in such proximity to their stars that they become tidally locked, resulting in a permanent day side and night side. Tidal locking occurs due to the gravitational force exerted by the star, which distorts the planet into an elongated shape. This results in synchronous rotation, where the planet's rotational period equals its orbital period (Barnes 2017).

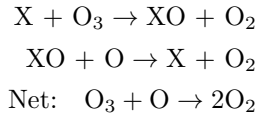
In addition to stellar properties, the habitable zone is significantly influenced by atmospheric composition, particularly the presence or absence of greenhouse gases. Ozone (O_3), acting as a greenhouse gas on Earth, influences the vertical temperature structure and humidity of the atmosphere. In absence of O_3 , the average surface temperature of an Earth-like planet would be 7K cooler (Gómez-Leal et al. 2019). Furthermore, O_3 serves as a filter for incoming UV radiation, safeguarding life on Earth's surface. Therefore, O_3 also plays a role in determining the potential habitability of an exoplanet.

To determine whether an exoplanet harbors life, scientists are keen on detecting biosignatures in its atmosphere. This detection can be achieved through direct imaging or transit spectroscopy. Direct imaging is particularly suitable for larger exoplanets in wider orbits around bright and massive stars. However, detecting small rocky planets through direct imaging poses a challenge due to the overshadowing effect of their host stars, especially with current technology, and also because habitable zones for M-dwarf stars are very close to them.

Scientists have considered using O_3 as a proxy to detect molecular oxygen (O_2) in the atmosphere of an exoplanet. However, a study conducted by Kozakis et al. (2022) has highlighted the challenge in accurately determining the amount of O_2 through O_3 measurements, especially when the UV flux of the host star is uncertain (Cooke et al. 2023). Nonetheless, if we have knowledge about the host star's UV spectrum and certain other information, O_3 measurements might offer insights into the potential habitability of an exoplanet.

On Earth O_3 is primarily produced in the tropical stratosphere via the Chapman mechanism (Chapman 1930). During daytime, UV radiation breaks the O_2 molecule to form two O atoms which then reacts with O_2 molecules and a third body M through a three-body process to form O_3 . The Brewer-Dobson circulation distributes O_3 in the stratosphere (Dobson 1956; Brewer 1949; Newell 1963). In this circulation pattern, air near the tropics rises and then moves toward the poles. The Brewer-Dobson circulation slightly differs between the two hemispheres due to variances in land and ocean structure in the Southern and the Northern hemispheres (Remsberg 2015).

This O_3 then either gets photodissociated by UV radiation to form O and O_2 , or it reacts with O to form two O_2 molecules. O_3 also gets catalytically destroyed by NO_x , HO_x , Br, Cl, etc (Portmann et al. 2012). If X is a catalytic species, then the O_3 is catalytically destroyed by the following reactions:



In 2016, three Earth-sized planets (TRAPPIST-1b, c, and d) were detected orbiting an ultra-cool M dwarf star known as TRAPPIST-1 or 2MASS J23062928 - 0502285, through observations made by the TRAPPIST (TRAnsiting Planets and PlanetIsimals Small Telescope) (Gillon et al. 2016). Subsequently, in 2017, Spitzer revealed the existence of four more exoplanets around TRAPPIST-1 (TRAPPIST-1e, f, g, and h), establishing it as the first system with seven Earth-sized planets (Gillon et al. 2017). All the planets in the TRAPPIST-1 system are closer to their host star than Mercury is to the Sun.

Future observations with JWST (Gardner et al. 2006) and new telescopes, such as ELT (Extremely Large Telescope) (Hook 2009) are expected to reveal more about small rocky exoplanets and their atmospheres. Looking ahead, future concepts like the Habitable Worlds Observatory (National Academies of Sciences, Engineering, and Medicine 2021), which was proposed by combining two earlier concepts - the HabEx (Habitable Exoplanet Observatory Mission) (Gaudi et al. 2020) and the LUVOIR (Large UV/Optical/IR Surveyor) (LUVOIR Team 2019) - are anticipated to directly image and characterize the atmospheres of Earth-like exoplanets. Hence, it becomes crucial to model rocky exoplanet atmospheres to aid in interpreting observations by extracting the atmospheric properties and explaining the underlying physical processes occurring in these exoplanetary atmospheres.

In previous studies, general circulation models (GCMs) have been employed to investigate the atmospheres of Earth-like planets, including studies designed to understand the atmospheric circulation and O₃ chemistry of tidally locked Earth-like exoplanets. For example, the TRAPPIST-1 Habitable Atmosphere Intercomparison (THAI) project (Turbet et al. 2022; Sergeev et al. 2022) compared the results from four GCMs which included slab oceans for both dry and moist N₂-dominated and CO₂-dominated atmospheres. Carone et al. (2018) used the MITgcm to study the stratospheric circulation of a tidally locked ExoEarth scenario for TRAPPIST-1b, TRAPPIST-1d, Proxima Centauri b and GJ 667 C f. Yates et al. (2020) employed the Met Office Unified Model to explore the O₃ chemistry of the tidally locked exoplanet Proxima Centauri b around an M dwarf, while Proedrou & Hocke (2016) used the CESM1(WACCM) model to simulate the 3D O₃ distribution of a tidally-locked Earth-like planet around a Sun-like star. A recent study conducted by Braam et al. (2023) utilized a slab ocean model of a tidally locked exoplanet around an M dwarf star with Proxima Centauri b parameters to study O₃ spatial distribution. They found that O₃ accumulates on the night side, demonstrating a day side-night side hemispheric asymmetry in O₃ distribution.

In our study we incorporated an Earth-like land-ocean structure to examine for the first time how orography might alter the atmospheric dynamics and chemistry of a TRAPPIST-1e exoplanetary atmosphere scenario. Our aim is to characterize the possible O₃ distribution and the influence of atmospheric circulation on it. We focus on O₃ because it is affected by photochemistry, catalytic cycles, atmospheric transport, and has strong spectral features from the UV to the mid-infrared. Additionally, the presence of O₂, a potential biosignature, can be inferred from a detection of O₃.

2. METHODS

2.1. *Model description and setup*

For this study, we modeled TRAPPIST-1e using the Whole Atmosphere Community Climate Model version 6 (WACCM6)(Gettelman et al. 2019). WACCM6 is an atmospheric model that operates as a configuration of the Community Earth System Model version 2 (CESM2). CESM2 is an Earth system model consisting of submodels simulating the atmosphere, ocean, land, sea ice, land ice, river runoff, and surface waves (Danabasoglu et al. 2020). The WACCM6 configuration comprises 70 vertical levels, starting from the surface at 1000 hPa and extending up to 140 km at 4.5×10^{-6} hPa (lower thermosphere), with a horizontal resolution of 1.875° latitude $\times 2.5^\circ$ longitude.

The chemistry applied in WACCM6 is based on the Model of Ozone and Related Chemical Tracers (MOZART). MOZART serves as a global chemical transport model encompassing physical and chemical processes that span the troposphere, stratosphere, mesosphere, and lower thermosphere (Emmons et al. 2020; Conley et al. 2012). WACCM6 employs the Rapid Radiative Transfer Model (RRTMG) radiation code for solving longwave (lower energy radiation emitted from the Earth's surface and atmosphere) and shortwave (higher energy wavelengths such as UV, visible light, and a part of the near-infrared spectrum, associated with the host star) radiative transfer equations.

WACCM6 has been previously utilized to study the climate and O₃ chemistry of prehistoric Earth and Earth-like exoplanets. For example, Cooke et al. (2022) demonstrated how the total O₃ column at O₂ concentrations between 0.1 - 50% the present atmospheric level, may have been lower than previously thought. The possible reasons behind this result are investigated in Ji et al. (2023). Cooke et al. (2023) showed how for an Earth-like exoplanet, observations and spectral signatures of chemical species could be affected by the line of sight, albedo, clouds, and chemistry. Liu et al. (2023) studied how changing the eccentricity of an Earth-like exoplanet affects the abundance and loss of water present in the atmosphere.

The model considered here used the BWma1850 compset³ of WACCM6, which included a pre-industrial Earth-like atmosphere and orography, and was modified to allow for synchronous rotation.⁴ The model composition was with O₂ set to present atmospheric level (PAL), i.e., 21% by volume, and N₂ with 78% by volume. The volume mixing ratios of CH₄ (0.8 ppmv), CO₂ (280 ppmv), N₂O (270 ppbv), and H₂ (500 ppbv), are fixed at the surface. We ran the simulation for 300 years, of which we utilised the last 40 years of data in order to eliminate any effects associated with the model adjusting to tidally-locked conditions. The substellar point was fixed at 180° longitude and 0° latitude over the Pacific Ocean (see Figure 1). Table 1 shows the parameters used to model TRAPPIST-1e. For this study, we have used a stellar spectrum based on the work of Peacock et al. (2019) who modelled the stellar energy distribution of TRAPPIST-1 and produced model 1A, 2A and 2B of which we used model 1A, which best matched the TRAPPIST-1 Ly α reconstruc-

³ <https://docs.cesm.ucar.edu/models/cesm2/config/2.1.3/compsets.html>

⁴ https://github.com/exo-cesm/CESM2.1.3/tree/main/Tidally_locked_exoplanets/cases

Parameter	Units	Value
Semimajor axis	au	0.029
Orbital period	Earth days	6.1
Rotation period	Earth days	6.1
Obliquity		0
Eccentricity		0
Instellation	W m^{-2}	900
Planet radius	km	5797
Gravity	m s^{-2}	9.14

Table 1. Planetary parameters used for model of TRAPPIST-1e (Grimm et al. 2018).

tion from Bourrier et al. (2017). Figure 2 compares the top-of-the-atmosphere irradiation of TRAPPIST-1e and Earth.

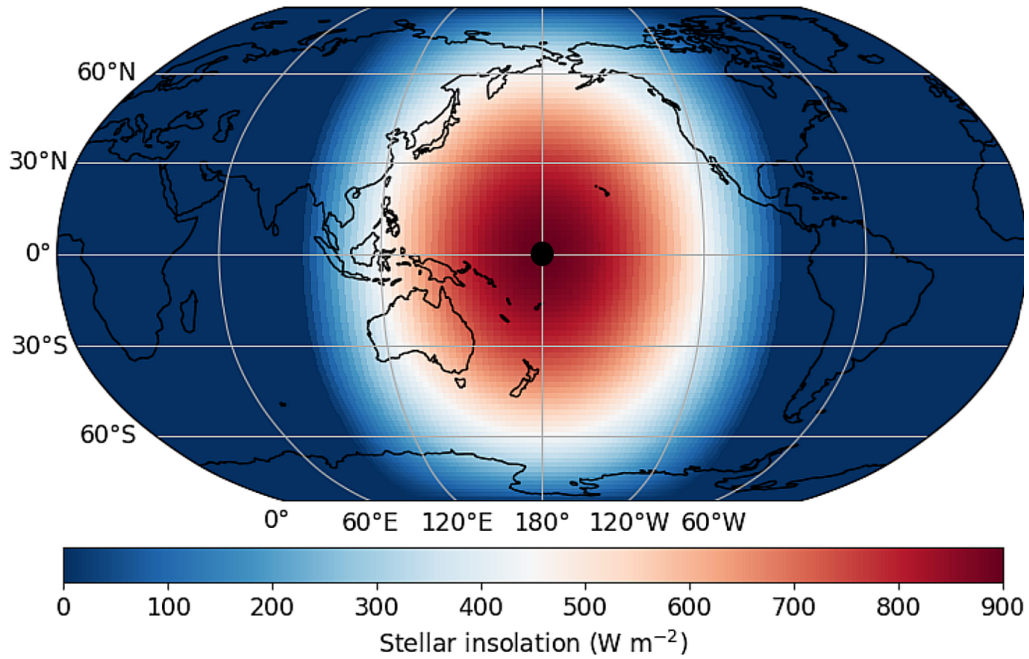


Figure 1. Stellar irradiation received by TRAPPIST-1e in our model. The black dot represent the substellar point which is fixed at 180° longitude and 0° latitude over the Pacific Ocean. The black outlines represent the land masses.

2.2. Data analysis

For our analysis, we calculated the time average of the 40 years of data and examined various parameters, including surface temperature, horizontal wind velocities (u and v), vertical wind velocity (w), reaction rates, and volume mixing ratios of O_3 , O_2 , OH , HO_2 , NO , NO_2 , Br , and Cl . To calculate the concentration of chemical species in units of molecules m^{-3} , we multiplied the air number density by the volume mixing ratio of the respective chemical species.

We calculated the O_x production rate using the formula $J_{\text{O}_2} * [\text{O}_2]$, where J_{O_2} is the oxygen photolysis rate constant and $[\text{O}_2]$ is the O_2 concentration. The catalytic destruction rates of O_3 by various chemical species (X) were calculated using the formula $k * [\text{X}] * [\text{O}_3]$, where k is the rate constant for $\text{X} + \text{O}_3$ reactions, $[\text{X}]$ is the concentration of the catalytic species, and $[\text{O}_3]$ is the concentration of O_3 . In this context, X can be OH , HO_2 , NO , NO_2 , Br , or Cl .

To study the horizontal wind circulation we used the Helmholtz wind decomposition, which has been previously used to study the atmospheric circulations of Earth, tidally locked terrestrial exoplanets and hot Jupiters (Hammond & Lewis 2021). The Helmholtz wind decomposition breaks down the total horizontal wind into rotational (\mathbf{u}_r) and

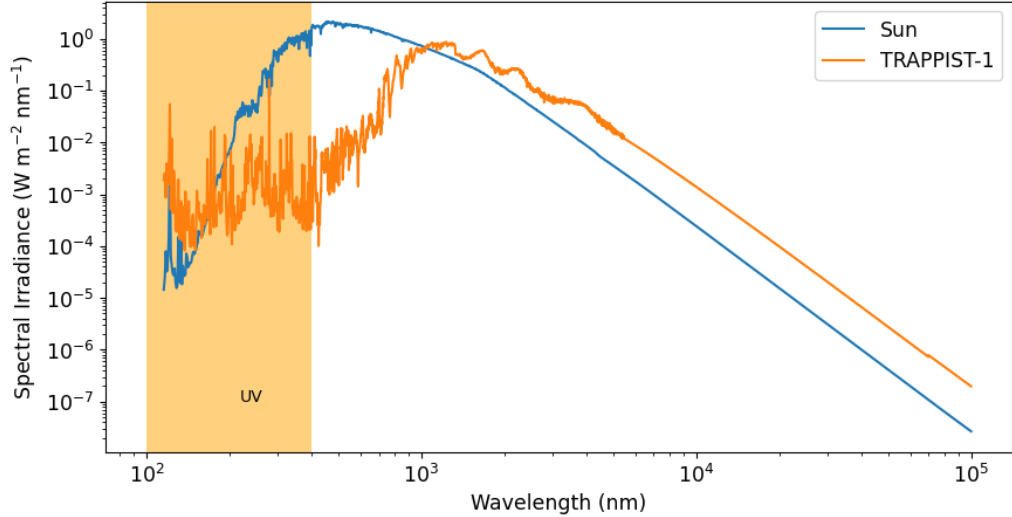


Figure 2. Stellar irradiance at top of the atmosphere of TRAPPIST-1e (orange) and Earth (blue). The orange shaded region represents the range of UV wavelengths.

divergent components (\mathbf{u}_d), allowing us to study the winds responsible for the overall circulation in more detail. For a tidally locked planet, the rotational flow consists of two parts: an equatorial jet (zonal-mean rotational component) which is a narrow belt of winds moving around the equator of a planet and stationary waves (eddy rotational component). The stationary waves drive the equatorial jet and can accelerate it resulting in a superrotating jet which moves faster than the planet's rotation rate (Showman et al. 2013). The divergent flow consists of a global overturning circulation which is a result of thermally driven circulation where the air rises on the day side of the planet and sinks on the night side. Mathematically, the Helmholtz wind decomposition divides the total circulation given by $\mathbf{u} = (u, v)$ into the two aforementioned components (Hammond & Lewis 2021):

$$\mathbf{u} = \mathbf{u}_d + \mathbf{u}_r = -\nabla\chi + \mathbf{k} \times \nabla\psi \quad (1)$$

$$\nabla^2\chi = \delta \quad (2)$$

$$\nabla^2\psi = \zeta \quad (3)$$

Here, \mathbf{u} represents the horizontal wind vector, where u and v denote the zonal (along latitude) and meridional (along longitude) velocities, respectively. The velocity potential function, χ , is derived from the divergence (δ - Equation 2), while the streamfunction, ψ , is derived from the vorticity (ζ - Equation 3) of the wind.

To examine the meridional overturning circulation, we used the meridional mass streamfunction. This is commonly used to study atmospheric or oceanic circulation patterns and helps in visualizing mass transport in the meridional plane (North-South direction). Mathematically, the relationship between mass streamfunction ψ and both vertical velocity (w) and meridional velocity (v) is expressed by the equations (Sidorenko et al. 2020)

$$\frac{1}{R} \frac{\partial\psi}{\partial\theta} = w, \quad \frac{\partial\psi}{\partial z} = -v \quad (4)$$

Here, θ is the latitude in radians, z is the altitude and R is the planet's radius.

3. RESULTS AND DISCUSSION

3.1. Ozone distribution

Figure 3 a) and b) show the O_3 concentration on the day and the night side of our TRAPPIST-1e model. O_3 is predominantly present in the lower atmosphere, below 10 hPa level (below ~ 30 km) and O_3 concentrations are higher near the poles than near the equator. The highest O_3 concentrations are found near the South pole between 600 and

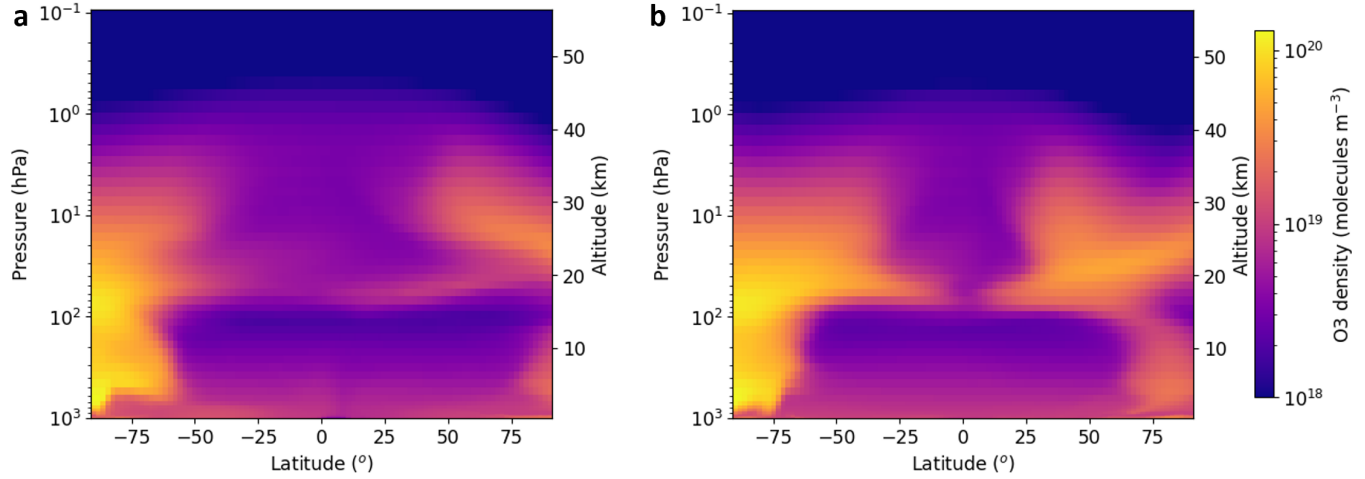


Figure 3. Cross section of the O_3 number density on the meridional plane passing through the a) substellar point and b) antistellar point for our TRAPPIST-1e model.

70 hPa levels (~ 5 and ~ 15 km). Further, there is little difference in O_3 concentrations between the day-side and the night-side, much less than the North-South asymmetry, suggesting that the O_3 produced on the day side is transported to the night side by horizontal winds.

Figure 4 a) and b) display the O_3 concentrations at 103 hPa (~ 15 km) and 609 hPa (~ 5 km) levels respectively. At both of these pressures, the North-South asymmetry in O_3 distribution is clearly visible. On Earth, O_3 is distributed in a roughly symmetrical manner about the equator, with the majority located between 300 and 10 hPa levels. Between 30 and 10 hPa levels, O_3 is densely packed around low latitudes, while between 300 and 30 hPa levels, O_3 is more abundant around the poles (see Ejzak et al. (2007)). Therefore, the vertical structure and the latitudinal distribution of O_3 in our TRAPPIST-1e model differs significantly from that of Earth.

Figure 5 shows the O_x production rate ($O + O_3$ production rate) on the meridional plane passing through the substellar point. The O_x production rate is symmetric, with peak production occurring in the upper atmosphere (above 10 hPa level or above ~ 30 km) due to the large amount of UV radiation received here. UV radiation does not penetrate the lower atmosphere because it becomes denser, absorbing most of the incoming UV radiation, and it is weakest at high latitudes due to geometric effects. Hence, in the lower atmosphere, there is less O_x production near the equator and no production at higher latitudes (as seen in figure 5, where white areas indicate regions of zero production). When comparing the pattern of O_3 concentration and O_x production rate, it is evident that the region of peak O_x production rate does not coincide with the region of peak O_3 concentration. There is relatively low O_3 concentrations where the O_x production is high, whereas the region with the highest O_3 concentration (near the South pole between 600 and 70 hPa levels) has either low or no O_x production. This indicates that O_3 is primarily produced high up in the atmosphere and either all the O_3 is transported from the upper atmosphere to the lower atmosphere, or some of it is transported while the remainder is catalytically destroyed. However, this does not explain the North-South asymmetry in O_3 concentration. To explain this asymmetry, we need to examine if there are asymmetries in catalytic species distribution and atmospheric circulation.

3.2. Role of catalytic species

Figure 6 shows the distribution of catalytic species (OH , HO_2 , NO , NO_2 , Cl , and Br) on the meridional plane passing through the substellar point for our TRAPPIST-1e model. For regions below 10 hPa level (~ 30 km), our initial hypothesis, after observing the symmetric O_x production and the asymmetric distribution of O_3 , was that there might be an uneven distribution of catalytic species. Such an imbalance could potentially be responsible for O_3 depletion being more pronounced near the North pole compared to the South pole. However, our analysis suggests that this is not the case, with the distribution of catalytic species being roughly symmetric and the concentrations low when compared to the O_3 concentration. In the case of Cl (Figure 6 e) and Br (Figure 6 f) we find that below 100 hPa level the concentrations of these species is slightly higher near the South pole as compared to the North pole, since

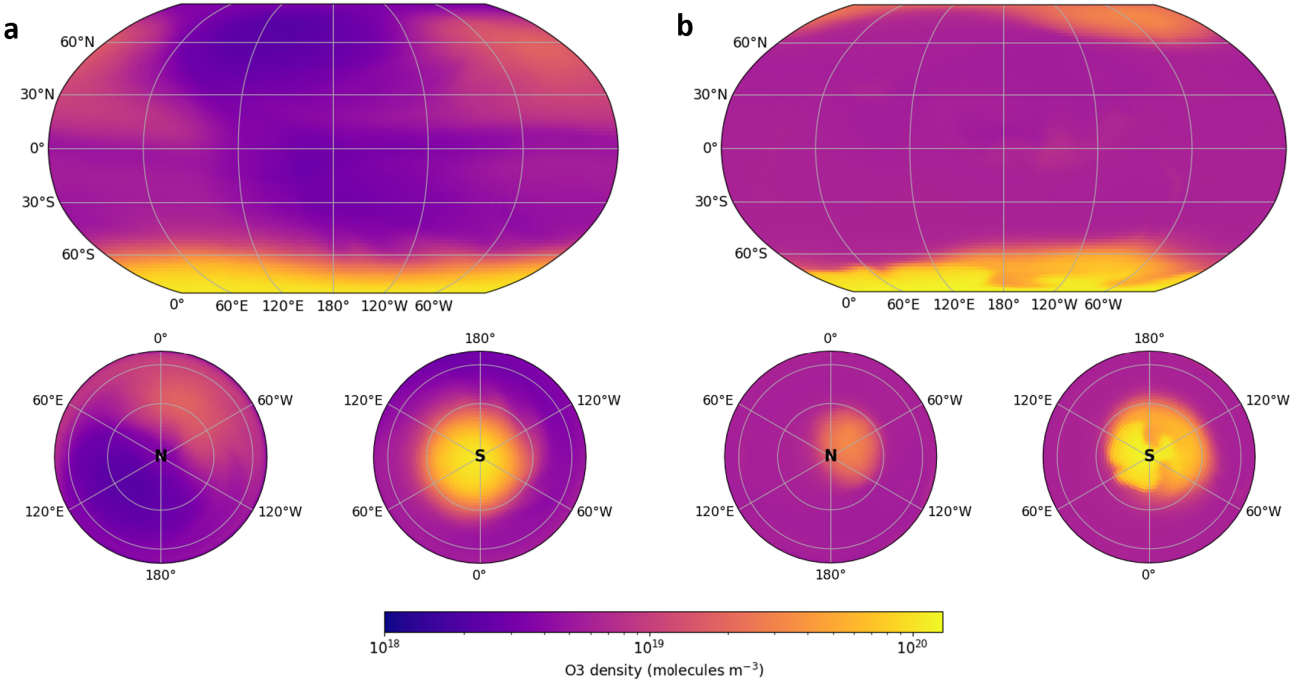


Figure 4. Horizontal slices of the O_3 number density for our TRAPPIST-1e model at a pressure (altitude) of a) 103 hPa (~ 15 km) and b) 609 hPa (~ 5 km). The substellar point is at 180° longitude and 0° latitude. N represents the North pole and S represents the South pole. Lower panels show the polar projections.

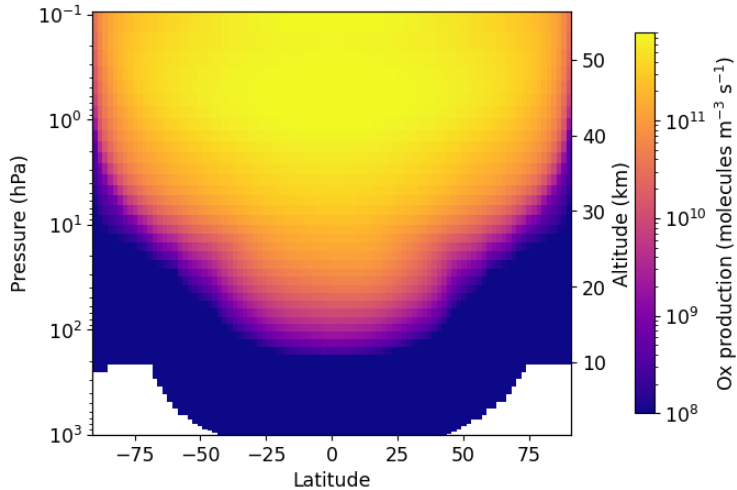


Figure 5. Cross section of O_x production rate on the meridional plane passing through the substellar point for our TRAPPIST-1e model. The white region on the plot indicates zero production rate.

this is aligned with the peak in ozone concentration, it cannot explain the high concentrations of O_3 we find below 10 hPa level near the South pole.

Figure 7 shows the time taken by the catalytic species to destroy O_3 on the day side. We observe that in the regions with the highest concentrations of O_3 , catalytic species require more time to destroy O_3 as compared to the regions where O_3 is produced. This observation implies that below the 10 hPa level, catalytic destruction proceeds at a slower rate, allowing sufficient time for atmospheric circulation to influence the distribution of O_3 . As such, this suggests that catalytic species may not be the primary factor driving the asymmetry in the distribution of O_3 . Therefore, we next look at the transport of O_3 throughout the atmosphere to see if this might have a more significant effect.

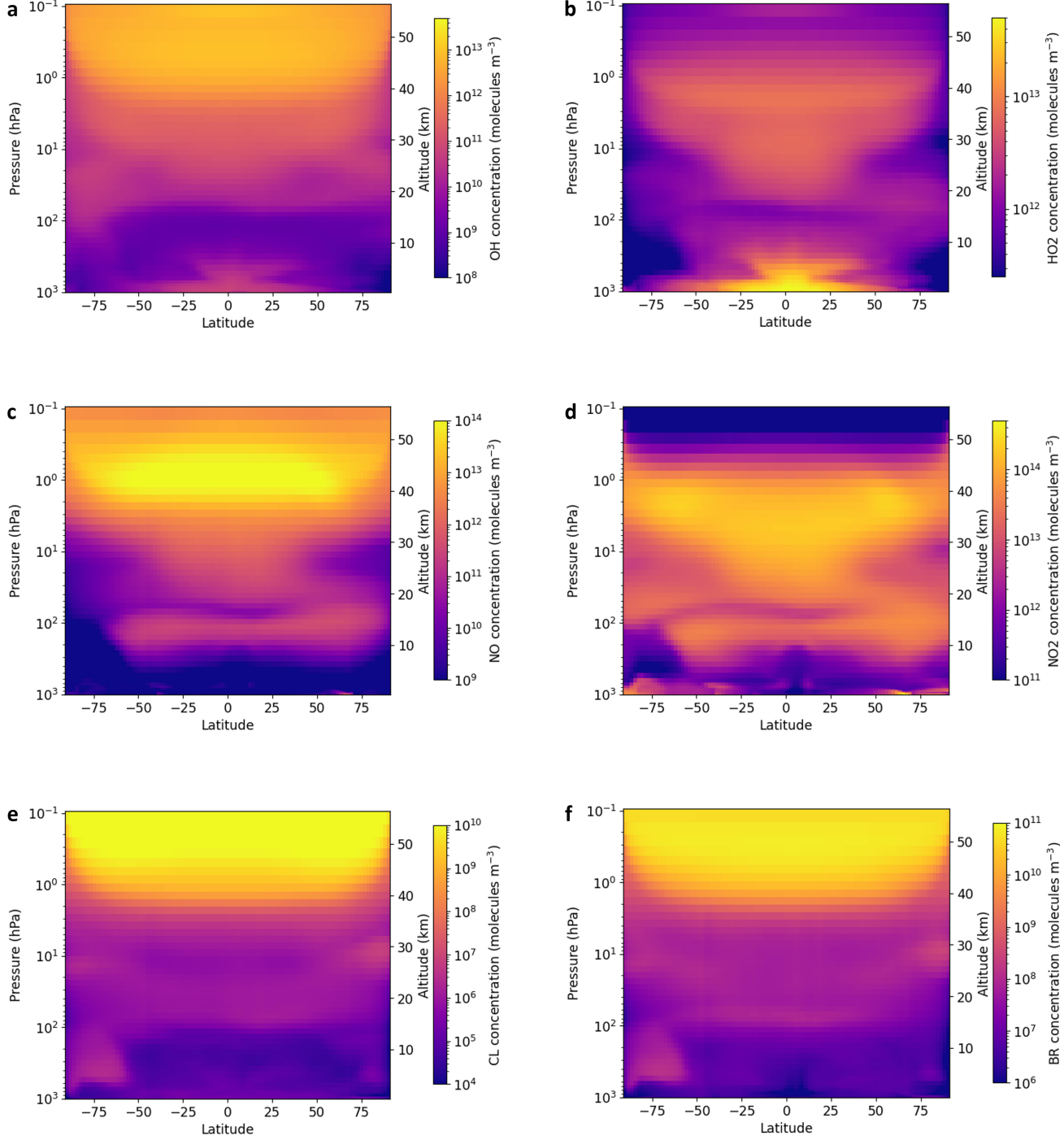


Figure 6. Catalytic species concentration on the meridional plane passing through the substellar point for a) OH, b) HO₂, c) NO, d) NO₂, e) Cl and f) Br for our TRAPPIST-1e model. The catalytic species are roughly symmetrically distributed and their concentrations are lower than the ozone concentrations.

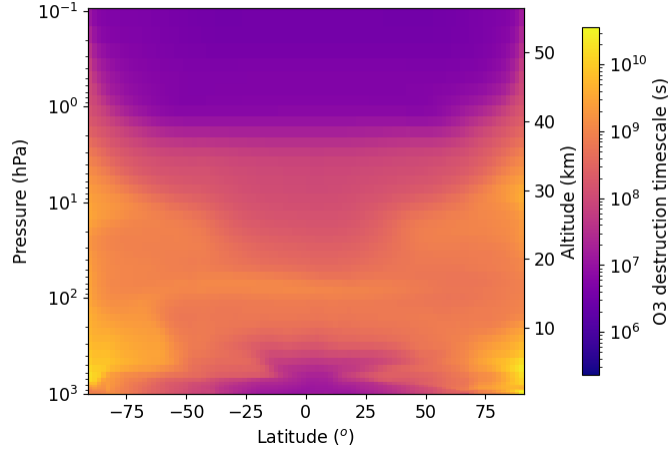


Figure 7. Time taken by the catalytic species to destroy O_3 on the meridional plane passing through the substellar point for our TRAPPIST-1e model.

3.3. *Role of atmospheric circulation*

Figure 8 a) and b) shows the meridional mass streamfunction on a plane passing through the substellar point and the antistar point, respectively. Here, red indicates clockwise transfer of mass and blue indicates anticlockwise transfer of mass. On the day side, without orography we would expect a symmetric circulation with upwelling at the equator, meridional flow towards the poles, downwelling near the poles and meridional flow from the poles to the equator (see Sergeev et al. (2022)). In our simulation, we find that there is an asymmetry in this circulation: near the North pole the downwelling is interrupted at 200 hPa level and does not reach the surface, rather there is a meridional transport from the North pole towards mid latitudes, downwelling at mid latitude and then meridional flow from mid latitude towards the equator (Figure 8 a). This asymmetry seems to be caused by the presence of a small anticlockwise (blue) circulation cell near the North pole. Similarly, on the night side, without orography we would expect to find upwelling near the poles, meridional transport from the poles to the equator, downwelling at the equator and meridional transport from the equator towards the poles near surface, thus closing the global overturning circulation (see Sergeev et al. (2022)). However, figure 8 b) reveals there is an asymmetry in this circulation. Near the North pole there are two circulation cells: below 200 hPa level, there is upwelling from the North pole, meridional transport from the North pole to the equator, downwelling near the equator until 200 hPa level, and meridional transport back to the North pole. Above 200 hPa level, there is downwelling near the North pole, meridional transport from the North pole, across the equator, to the South pole, and then upwelling near the South pole.

So, both on the day side and night side we find an asymmetry in the meridional overturning circulation, near the North pole due to the presence of a small anticlockwise circulation cell on the day side and a large clockwise circulation cell on the night side. This asymmetry is caused by the presence of Earth-like orography. Both on the day side and the night side the Northern hemisphere has higher fraction of land mass as compared to the Southern hemisphere. This landmass helps to reshape the wind, leading to the asymmetric meridional overturning circulation near the North pole.

The horizontal flow is complex, but the Helmholtz wind decomposition gives us an easier way to understand it. Figure 9 and Figure 10 show the divergent component and the eddy rotational component of the horizontal winds in the stratosphere (20 hPa level), near the tropopause (103 hPa level), and near the surface (800 hPa level). When comparing the mean wind speeds of both components at each pressure level, we find that the eddy rotational component has a higher mean wind speed than the divergent component. This implies that the eddy rotational component plays a major role in meridional transport.

We can explain the O_3 concentrations North-South asymmetry using both the meridional overturning circulation and the Helmholtz wind decomposition. O_3 formed on the day side between 200 and 10 hPa levels (~ 10 and ~ 30 km) is evenly transported toward the poles by meridional flow and then from the day side to the night side by the rotational component of horizontal winds, which includes both the eddy and zonal-mean components. On the night side, in the lower atmosphere (below 100 hPa level), the meridional flow (see Figure 10 c) forces large amounts of O_3

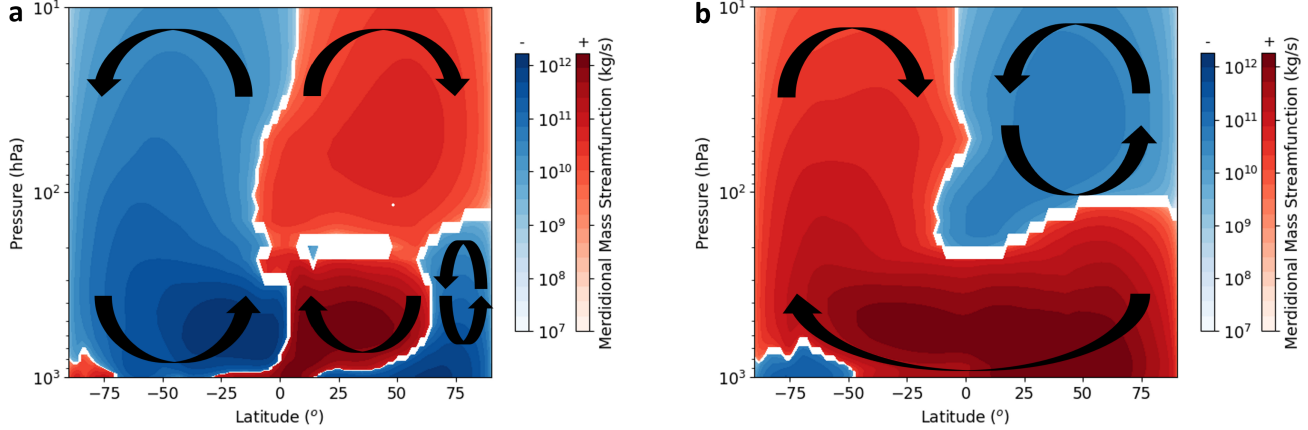


Figure 8. Meridional mass streamfunction on the meridional plane passing through the a) substellar point and the b) antistar point for our TRAPPIST-1e model. The positive values (red) indicates clockwise circulation and the negative values (blue) indicates anticlockwise circulation. The values are in log-scale.

from the North pole to the South pole. The North-South asymmetry on the night side in the meridional flow, near the surface, occurs due to the presence of Earth-like orography. Land-ocean boundaries cause wave breaking (not shown), resulting in a flow from the North pole towards the South pole disrupting the symmetric day/night transport found by Braam et al. (2023). Also, near the North pole, below 100 hPa level, the presence of a small anticlockwise circulation cell on the day side and large clockwise circulation cell on the night side in the lower atmosphere, prevents O₃ from accumulating at higher latitudes.

Considering, Figure 5 and Figure 10 a) and b), we find that the O₃ formed at the substellar point between 200 and 10 hPa levels (~ 10 and ~ 30 km) is first pushed towards the 120° longitude, then towards the poles, and from the day side to the night side by the rotationally driven winds. Below 200 hPa level (~ 30 km) on the night side (300° – 360° longitude), the flow from the North pole to the South pole (see Figure 10 c) forces O₃ towards the South pole which then gets well mixed by the rotational component of the horizontal winds resulting in high O₃ concentrations in the lower atmosphere near the South pole on both the day side and the night side.

3.4. Total ozone column density of TRAPPIST-1e and Earth

Total ozone column (TOC) density is reported in Dobson Units (DU), where 1 DU is equivalent to a 10 μ m thick layer of pure O₃ at 273 K and 1 atm pressure. For Earth the values of TOC are 200-250 DU near the South pole and 300-350 DU near the North pole.⁵ Figure 11 shows the latitudinal variation in zonal mean TOC density for TRAPPIST-1e and Earth. From this figure, we clearly observe the North-South asymmetry in O₃ distribution for our TRAPPIST-1e model, whereas O₃ on Earth is roughly symmetrically distributed about the equator. It is also interesting to note that the total O₃ concentration on TRAPPIST-1e is much higher compared to that of Earth. The TOC density on TRAPPIST-1e near the South pole is 8000 DU, which is around 28 times that of Earth (~ 250 DU), and near the North pole, it is approximately 2000 DU, which is 7 times that of Earth (~ 300 DU). There is slight asymmetry in TOC on Earth with slightly higher TOC near the North pole as compared to the South pole, but for TRAPPIST-1e this asymmetry is reversed, and significantly larger.

From our results we can say that TRAPPIST-1e has the potential to exhibit large O₃ concentrations, which could be potentially observable. Furthermore, if O₃ is detected, this would be indicative of atmospheric oxygen. Chen et al. (2019) demonstrated through simulated transmission spectra of M-dwarf planets that JWST could potentially detect O₃ features during primary transit. However, detecting the prominent O₃ features would require over 100 transits in conditions of zero cloud coverage, and twice that number in instances of 100% cloud coverage (Lustig-Yaeger et al. 2019). There are numerous factors which influence the O₃ spectral signature, such as the line of sight of the telescope

⁵ <https://ozonewatch.gsfc.nasa.gov/SH.html> - Date: 24/08/2023

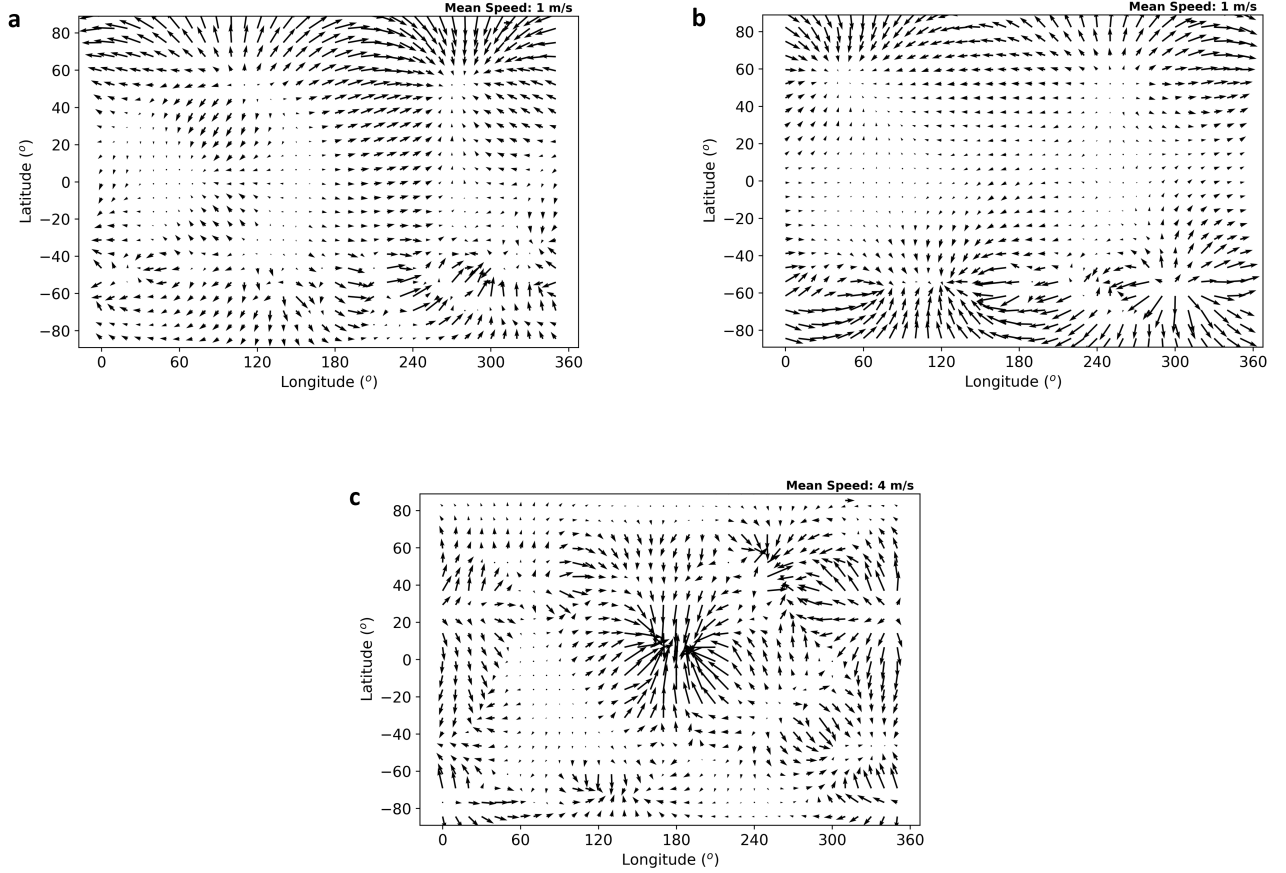


Figure 9. Helmholtz divergent winds at a) 20 hPa, b) 103 hPa and c) 800 hPa levels. Arrows represents winds velocity vectors and point in the direction of flow, with the length of the arrows representing the magnitude of the wind speed (with the mean wind speed shown in the top right corner of each plot).

and the presence of other chemical species (Proedrou & Hocke 2016). The brightness of an exoplanet changes as it orbits its host star and is depicted by the full-phase light curve. This curve shows the entire range of phases from minimum to maximum illumination (Seager 2010). The presence of land and ocean masses can lead to non-uniform O₃ distributions as found in our model and hence as the planet orbits its host star, the amounts of O₃ that is visible might also change. Hence, the detection of O₃ might depend on the phase of the exoplanet we observe. The presence of other chemical constituents in the atmosphere could also hinder O₃ detection by affecting its spectral signature. Chemical constituents which have similar spectral features to O₃ could overlap with an O₃ spectral features making it difficult to detect O₃. Finally, TRAPPIST-1 is a highly active star with dark spots and bright faculae on its surface which could make O₃ detection difficult by interfering with the transmission spectrum of the planet (Lim et al. 2023).

3.5. Limitations and Future Work

The limitation of our study is that we considered an Earth-like orography and atmospheric composition, which is likely not to be the case in reality. Slab ocean are also unlikely to be physical. In a follow up study we would like to look into detail how the land structures disrupts the near surface winds. We would also like to study how changing the location of the substellar point (with respect to the land-mass distribution) affects the distribution and overall concentration of O₃, atmospheric dynamics and chemistry and how would these might influence observations.

4. SUMMARY

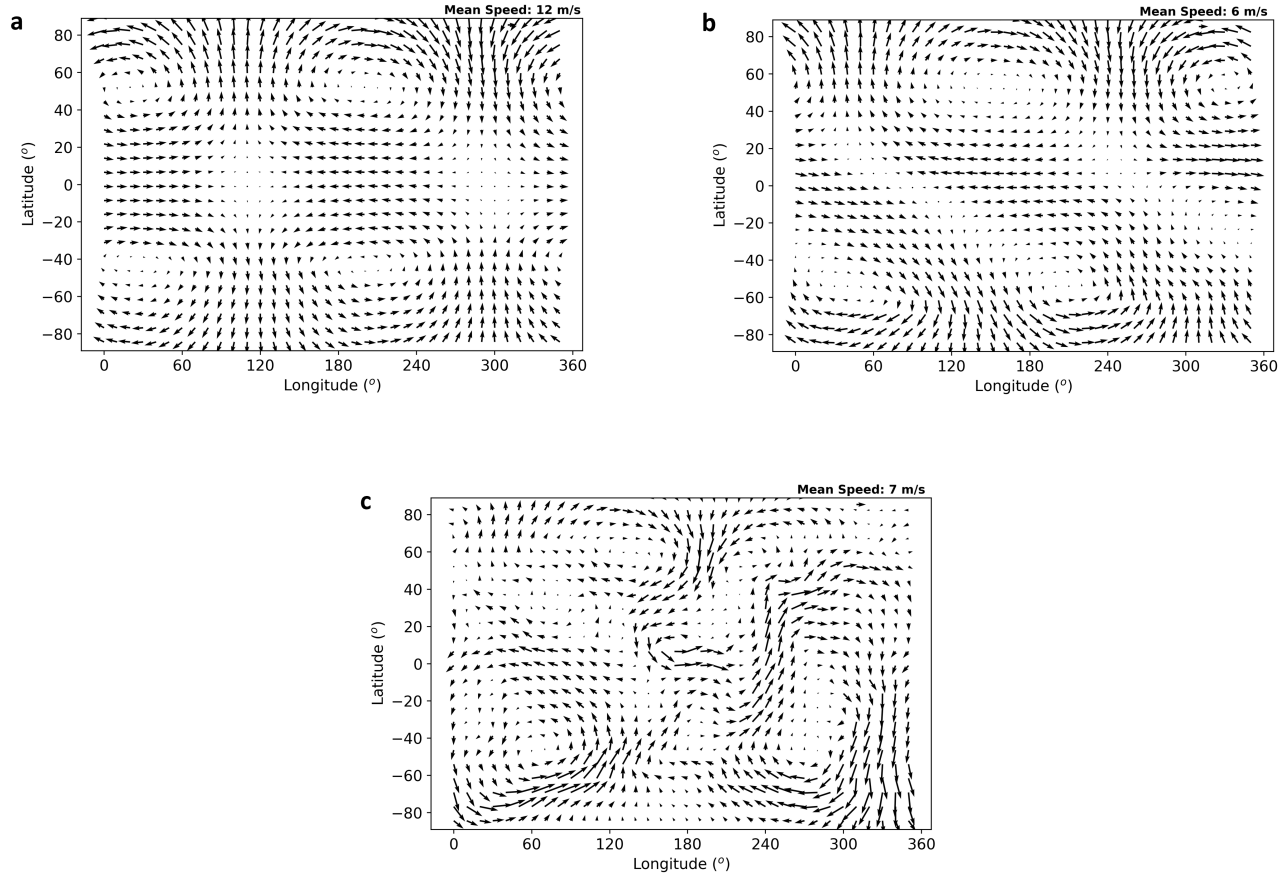


Figure 10. Helmholtz rotational eddy winds at a) 20 hPa, b) 103 hPa and c) 800 hPa. Arrows represent winds velocity vectors and point in the direction of flow, with the length of the arrows representing the magnitude of the wind speed (with the mean wind speed shown in the top right corner of each plot).

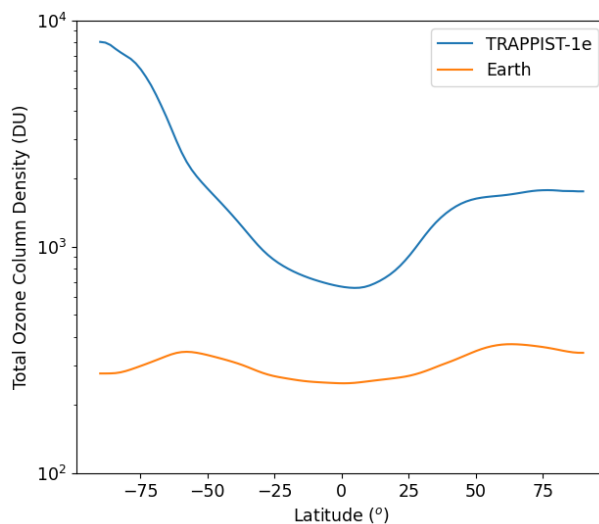


Figure 11. Zonal mean latitudinal variation of total ozone column density for our TRAPPIST-1e model (blue) and Earth (orange).

In this study we used the CESM2-WACCM6 GCM which includes Earth-like orography to simulate the tidally locked exoplanet TRAPPIST-1e and investigate the O_3 distribution and how the atmospheric circulations shape it. The atmospheric composition was set to pre-industrial Earth-like composition (O_2 - N_2 dominated). The substellar point was positioned over the ocean at 180° longitude and 0° latitude, and the stellar irradiance was based on the TRAPPIST-1 spectrum of Peacock et al. (2019). We analyzed the time average of 40 years of steady state simulation data for our study.

Our results reveal a North-South asymmetry in O_3 distribution. O_3 is highly concentrated near the South pole below 10 hPa level (below ~ 30 km). This does not relate to O_x production, which is symmetric at low pressures and is least prevalent in the deep atmosphere, especially near the poles. On the day side, O_x generation is symmetrical and reaches its peak above 10 hPa level (above ~ 30 km). Below 10 hPa level (below ~ 30 km), O_x production is minimal in low latitudes and lacking or minimal in high latitudes. This suggests that where high O_3 concentrations exist, O_x production is either significantly reduced or entirely absent. On examining the distribution of catalytic species (OH, HO_2 , NO, NO_2 , Br, and Cl) we found a relatively symmetrical distribution. This suggests that catalytic destruction is not primarily responsible for asymmetric O_3 distribution.

Consequently we next investigated if O_3 transport is responsible for the O_3 asymmetry. Indeed after examining the atmospheric circulation patterns, we identified an asymmetry in the meridional overturning circulation near the North pole. This discrepancy is caused by wave breaking due to land-ocean boundaries, impacting near surface winds and resulting in a flow from the North pole to the South pole on the night side. Analyzing the Helmholtz wind decomposition revealed that the rotational component, specifically the eddy wind component dominated over the divergent component of the wind i.e. the wave driven transport dominates the global overturning circulation.

Upon comparing meridional circulation on the day side with O_x production, we observed that O_3 generated above 10 hPa level (above ~ 30 km) near low latitudes is carried towards the poles by this circulation. Subsequently, horizontal winds (linked with the rotational component) carry O_3 from the day side to the night side below 100 hPa level (below ~ 10 km) and on the night side, a North-to-South flow near the surface forces O_3 near the South pole which gets distributed zonally by a wind gyre at the South pole. The eddy winds which drives the meridional transport is what leads to asymmetry in the observed meridional overturning circulation and O_3 distribution.

The asymmetry in O_3 distribution for our TRAPPIST-1e model is intriguing. On Earth, O_3 is distributed by the Brewer-Dobson circulation, leading to an O_3 distribution that is approximately symmetric about the equator. However, in our TRAPPIST-1e model, the combination of tidal locking and the inclusion of the Earth-like orography generates an asymmetric circulation pattern, leading to O_3 asymmetry. Our TRAPPIST-1e model was found to exhibit a higher TOC density than Earth with 8000 DU, nearly 28 times higher than Earth near the South pole, and 2000 DU, which is roughly 7 times higher than Earth near the North pole. It is interesting how tidal locking and orography affects the global overturning circulation and O_3 chemistry.

F. Sainsbury-Martinez would like to thank UK Research and Innovation for support under grant number MR/T040726/1. G.J.C. acknowledges the studentship funded by the Science and Technology Facilities Council of the United Kingdom (STFC; grant number ST/T506230/1). This work was undertaken on ARC4, part of the High Performance Computing facilities at the University of Leeds, UK.

REFERENCES

Barnes, R. 2017, Celestial Mechanics and Dynamical Astronomy, 129, 509

Bochanski, J. J., Hawley, S. L., Covey, K. R., et al. 2010, The Astronomical Journal, 139, 2679, doi: [10.1088/0004-6256/139/6/2679](https://doi.org/10.1088/0004-6256/139/6/2679)

Bourrier, V., Ehrenreich, D., Wheatley, P., et al. 2017, Astronomy & Astrophysics, 599, L3

Braam, M., Palmer, P., & Decin, L. 2023, in EGU General Assembly Conference Abstracts, EGU General Assembly Conference Abstracts, EGU-15501, doi: [10.5194/egusphere-egu23-15501](https://doi.org/10.5194/egusphere-egu23-15501)

Brewer, A. 1949, Quarterly Journal of the Royal Meteorological Society, 75, 351

Carone, L., Keppens, R., Decin, L., & Henning, T. 2018, MNRAS, 473, 4672, doi: [10.1093/mnras/stx2732](https://doi.org/10.1093/mnras/stx2732)

Chapman, S. 1930, Mem. Roy. Meteor. Soc., 3, 103

Chen, H., Wolf, E. T., Zhan, Z., & Horton, D. E. 2019, The Astrophysical Journal, 886, 16, doi: [10.3847/1538-4357/ab4f7e](https://doi.org/10.3847/1538-4357/ab4f7e)

Conley, A. J., Garcia, R., Kinnison, D., et al. 2012, NCAR technical note, 3

Cooke, G., Marsh, D., Walsh, C., Black, B., & Lamarque, J.-F. 2022, A revised lower estimate of ozone columns during Earth's oxygenated history. <https://arxiv.org/abs/2102.11675>

Cooke, G., Marsh, D., Walsh, C., & Youngblood, A. 2023, Degenerate interpretations of O₃ spectral features in exoplanet atmosphere observations due to stellar UV uncertainties: a 3D case study with TRAPPIST-1e

Cooke, G. J., Marsh, D. R., Walsh, C., Rugheimer, S., & Villanueva, G. L. 2023, MNRAS, 518, 206, doi: [10.1093/mnras/stac2604](https://doi.org/10.1093/mnras/stac2604)

Danabasoglu, G., Lamarque, J.-F., Bacmeister, J., et al. 2020, Journal of Advances in Modeling Earth Systems, 12, e2019MS001916

Dobson, G. M. B. 1956, Proceedings of the Royal Society of London. Series A. Mathematical and Physical Sciences, 236, 187

Dressing, C. D., & Charbonneau, D. 2015, The Astrophysical Journal, 807, 45

Ejzak, L. M., Melott, A. L., Medvedev, M. V., & Thomas, B. C. 2007, The Astrophysical Journal, 654, 373, doi: [10.1086/509106](https://doi.org/10.1086/509106)

Emmons, L. K., Schwantes, R. H., Orlando, J. J., et al. 2020, Journal of Advances in Modeling Earth Systems, 12. <https://api.semanticscholar.org/CorpusID:216525929>

Gaidos, E., Mann, A., Kraus, A., & Ireland, M. 2016, Monthly Notices of the Royal Astronomical Society, 457, 2877

Gardner, J. P., Mather, J. C., Clampin, M., et al. 2006, Space Science Reviews, 123, 485, doi: [10.1007/s11214-006-8315-7](https://doi.org/10.1007/s11214-006-8315-7)

Gaudi, B. S., Seager, S., Mennesson, B., et al. 2020, The Habitable Exoplanet Observatory (HabEx) Mission Concept Study Final Report. <https://arxiv.org/abs/2001.06683>

Gettelman, A., Mills, M., Kinnison, D., et al. 2019, Journal of Geophysical Research: Atmospheres, 124, 12380

Gillon, M., Jehin, E., Lederer, S. M., et al. 2016, Nature, 533, 221, doi: [10.1038/nature17448](https://doi.org/10.1038/nature17448)

Gillon, M., Triaud, A. H. M. J., Demory, B.-O., et al. 2017, Nature, 542, 456, doi: [10.1038/nature21360](https://doi.org/10.1038/nature21360)

Gómez-Leal, I., Kaltenegger, L., Lucarini, V., & Lunkeit, F. 2019, Icarus, 321, 608, doi: [10.1016/j.icarus.2018.11.019](https://doi.org/10.1016/j.icarus.2018.11.019)

Gould, A., Pepper, J., & DePoy, D. 2003, The Astrophysical Journal, 594, 533

Grimm, Demory, Brice-Olivier, Gillon, Michaël, et al. 2018, A&A, 613, A68, doi: [10.1051/0004-6361/201732233](https://doi.org/10.1051/0004-6361/201732233)

Hammond, M., & Lewis, N. T. 2021, Proceedings of the National Academy of Sciences, 118, doi: [10.1073/pnas.2022705118](https://doi.org/10.1073/pnas.2022705118)

Hook, I. 2009, in Science with the VLT in the ELT Era, Springer, 225–232

Howard, A. W., Marcy, G. W., Bryson, S. T., et al. 2012, The Astrophysical Journal Supplement Series, 201, 15

Huang, S.-S. 1959, Publications of the Astronomical Society of the Pacific, 71, 421

Ji, A., Kasting, J. F., Cooke, G. J., Marsh, D. R., & Tsigaris, K. 2023, Roy. Soc. Open Sci., 10, 230056, doi: [10.1098/rsos.230056](https://doi.org/10.1098/rsos.230056)

Kozakis, T., Mendonça, J. M., & Buchhave, L. A. 2022, Astronomy and Astrophysics, 665, A156, doi: [10.1051/0004-6361/202244164](https://doi.org/10.1051/0004-6361/202244164)

Lim, O., Benneke, B., Doyon, R., et al. 2023, ApJL, 955, L22, doi: [10.3847/2041-8213/acfc4](https://doi.org/10.3847/2041-8213/acfc4)

Liu, B., Marsh, D. R., Walsh, C., & Cooke, G. 2023, MNRAS, 524, 1491, doi: [10.1093/mnras/stad1828](https://doi.org/10.1093/mnras/stad1828)

Lustig-Yaeger, J., Meadows, V. S., & Lincowski, A. P. 2019, The Astronomical Journal, 158, 27, doi: [10.3847/1538-3881/ab21e0](https://doi.org/10.3847/1538-3881/ab21e0)

LUVOIR Team. 2019, The LUVOIR Mission Concept Study Final Report. <https://arxiv.org/abs/1912.06219>

Mulders, G. D., Pascucci, I., & Apai, D. 2015, The Astrophysical Journal, 814, 130

National Academies of Sciences, Engineering, and Medicine. 2021, Decadal survey on astronomy and astrophysics 2020, The National Academies Press Washington, DC

Newell, R. E. 1963, Quarterly Journal of the Royal Meteorological Society, 89, 167

Nutzman, P., & Charbonneau, D. 2008, Publications of the Astronomical Society of the Pacific, 120, 317

Peacock, S., Barman, T., Shkolnik, E. L., Hauschildt, P. H., & Baron, E. 2019, The Astrophysical Journal, 871, 235

Portmann, R., Daniel, J., & Ravishankara, A. 2012, Philosophical Transactions of the Royal Society B: Biological Sciences, 367, 1256

Proedrou, E., & Hocke, K. 2016, Earth, Planets and Space, 68, 1

Reiners, A., Zechmeister, M., Caballero, J., et al. 2018, Astronomy & Astrophysics, 612, A49

Remsberg, E. 2015, Atmospheric Chemistry and Physics, 15, 3739, doi: [10.5194/acp-15-3739-2015](https://doi.org/10.5194/acp-15-3739-2015)

Seager, S. 2010, Exoplanets

Sergeev, D. E., Fauchez, T. J., Turbet, M., et al. 2022, The Planetary Science Journal, 3, 212

Shields, A. L., Ballard, S., & Johnson, J. A. 2016, Physics Reports, 663, 1

Showman, A. P., Wordsworth, R. D., Merlis, T. M., & Kaspi, Y. 2013, in Comparative Climatology of Terrestrial Planets (University of Arizona Press), doi: [10.2458/azu_uapress_9780816530595-ch12](https://doi.org/10.2458/azu_uapress_9780816530595-ch12)

Sidorenko, D., Danilov, S., Koldunov, N., Scholz, P., & Wang, Q. 2020, Geoscientific Model Development, 13, 3337, doi: [10.5194/gmd-13-3337-2020](https://doi.org/10.5194/gmd-13-3337-2020)

Turbet, M., Fauchez, T. J., Sergeev, D. E., et al. 2022, The Planetary Science Journal, 3, 211

Yates, J. S., Palmer, P. I., Manners, J., et al. 2020, Monthly Notices of the Royal Astronomical Society, 492, 1691